Agnès Maurel & Philippe Petitjeans

Vortex Structure and Dynamics, Edition

SPIN Springer's internal project number, if known

Springer

Berlin Heidelberg New York

Barcelona Budapest Hong Kong

London Milan Paris

Santa Clara Singapore Tokyo

Acoustic Characterization of a Stretched Vortex in an Infinite Medium

Sébastien Manneville[1], Agnès Maurel[1], Frédéric Bottausci[2]
and Philippe Petitjeans[2]

[1] Laboratoire Ondes et Acoustique, UMR CNRS 7587 ESPCI, 10 rue Vauquelin, 75005 Paris, France
[2] Laboratoire Physique et Mécanique des Milieux Hétérogènes, UMR CNRS 7636, ESPCI, 10 rue Vauquelin, 75005 Paris, France

Abstract. A new experimental device is presented, that allows to isolate and control a stretched vortex in an "infinite" medium. Acoustic measurements based on the ultrasound-flow interaction yield the main vortex characteristics (position, circulation, core size). This global and non-invasive method also allows a dynamical tracking of the vortex. Experimental results on the mean vortex characteristics as a function of the control parameters are presented, together with some examples of transitory regimes and of precession motion.

1 Introduction

Experimental measurements of the vorticity and of the dynamics of vortical structures in fluid flows are essential to the understanding of hydrodynamic instabilities and, more generally, of turbulence. Indeed, in turbulent flows, experimental observations [2] as well as numerical simulations [2,3] have revealed the presence of very intense rotational structures that concentrate most of the vorticity of the flow. Such structures of small diameter but very long along their rotation axis often display a strong "stretching" (large longitudinal velocity gradients).

In general, it is almost impossible to isolate those "vorticity filaments" from the surrounding turbulent flow and their role in small scale intermittency in turbulence is not yet clearly understood [4,5,7]. That's why many recent experiments try and create isolated stretched vortices in various geometries [8–11], mostly inspired from Von Kármán flows generated between two rotating discs in a confined medium. To break free from restrictive boundary conditions, we set up a new experimental device that allows to control a stretched vortex in an "infinite" medium. This device is described in the next section.

To avoid the use of a probe or the seeding of the flow like in classical measurement techniques (hot wire anemometry, Laser Doppler Velocimetry, dye or particles flow visualization, Ultrasound Doppler Velocimetry), we tested a new acoustic technique to measure the vortex characteristics [12,3,14,15]. This technique based on the sound-flow interaction is briefly recalled in the third section.

The last section of this paper shows the experimental results. In particular, the acoustic measurement tool is shown to provide a thorough characterization of a very strongly stretched vortex in both its mean behaviour and its dynamics.

2 Experimental setup

A stretched vortex is generated in water between two identical rotating discs by applying a pumping at the center of each disc. In this experiment, rotation and stretching are thus applied independently and at the same points by rotating tubing. The rotation frequency $\Omega/2\pi$ is fixed by a feedback motor (Yaskawa DR2 Servopack) and tunable between 0 and 25 Hz. In the experiments presented below, the disc radius is 10 cm and the discs are corotating along the same axis.

Suction is applied at the center of each disc through a small hole of diameter 5 mm by a pump (Eheim IP67). The suction flowrate Q is set by a gate controlled by a step-by-step motor and ranges from 0 to 6.4 L/min. In our experiments, the pumping is symmetrical so that the flowrate for each disc ranges from 0 to 3.2 L/min, which corresponds to longitudinal velocities up to 5 m/s at the suction holes. To avoid stirring of the surrounding fluid, the rotating tubing is inserted into fixed PVC tubing.

The initial vorticity generated by the discs is amplified by the pumping [11] and this setup gives birth to a very intense stretched vortex ("vorticity filament"). Its length, which is also the distance D between the two discs, can be tuned up to about 30 cm. The large volume of the water tank (300 L) allows us to neglect the effects of the boundaries on the vortex: in the experiments described below, the nearest wall is 20 cm away from the vortex and the free surface is at 30 cm. Unlike experiments in cylindrical geometries [10][12][16] where the disc diameter is about the size of the water tank, boundary conditions -except those on the discs- are of no influence in the present experiment.

Figure 1 shows two photographs of the vortex visualized by injecting a dye directly in the vortex core . Most of the time, the vortex appears as a straight filament linking the centers of the two discs (fig. 1(a)). Depending on the control parameters, the vortex also follows a small precession motion around the rotation axis of the discs. Observations also show large fluctuations of the "stagnation point" (point on the vortex axis where the longitudinal velocity v_z is zero) and even a layered radial structure of v_z and of the stretching $\partial v_z/\partial z$.

During transitory regimes (formation of the vortex, vortex breakdown after a perturbation or depending on the experimental conditions), the vortex can undergo large deviations far from the rotation axis of the discs (fig. 1(b)). In such cases, transitory precession motions of large amplitude are observed, followed by a relaxation towards a more stable state.

3 Acoustic measurement of the vortex characteristics

Even if Doppler methods (Laser or Ultrasound Doppler Velocimetry) avoid placing a probe inside the vortex core, those methods require that the flow be seeded by scatterers. The dynamics of such scatterers in a vorticity filament was shown to be very complex and to give rise to demixtion phenomena where the scatterers migrate towards low pressure areas [18]. Moreover, the size of the measurement volume in Doppler techniques is sometimes too large as compared to the size of the vortex filament, which restricts the precision in the vortex core.

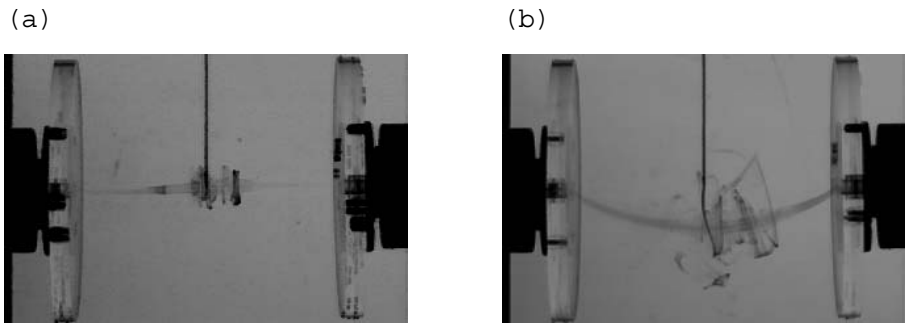

Fig. 1. Visualization of the vortex generated by the "double rotating suction system". (a) Stable regime. (b) Large departure from the rotation axis of the discs during the transitory regime of formation of the vortex. The dark line in the middle of the picture corresponds to the dye injector.

Our measurement method relies on the transmission of an ultrasonic wave in a moving medium without seeding and derives from classical acoustic tomography techniques used in oceanography for instance [19,20] .

3.1 The sound-flow interaction

An acoustic wave that crosses a moving medium is advected and distorted by the flow velocity field. If geometrical acoustics are valid, that is when the flow is slowly varying in space compared to the acoustic wavelength λ, the distortion simply results from a velocity composition: the wave is either sped up or slowed down depending on the area of the flow it crosses (see fig. 2). In that case, the ray theory for acoustic propagation can be used and many authors have investigated the trajectories of acoustic rays in a vortex [21–23]. Experiments on "large" vortices -with a characteristic size much larger than λ- [3,14] have shown the importance of geometric distortions of an acoustic wavefront due to a vortex and confirmed that fully non-invasive measurements of its characteristics were possible.

In the opposite limit where the fluid velocity field has strong velocity gradients localized on sizes smaller than λ, the incident wave is scattered by the flow. The theoretical framework provided by the Born approximation has led to numerous studies on sound scattering by a vortex [24–28] to predict the pressure field radiated far from an isolated vortex or from a turbulent flow modelled by a random gas of vortices. Experimentally, those studies triggered the first vorticity measurements by scattering of sound in hydrodynamics [29–31].

In our experiment, the order of magnitude of the control parameters lead to a vortex whose core is only a few λ so that the experimental situation is in between the two limits presented above and mixes both geometric effects and sound scattering.

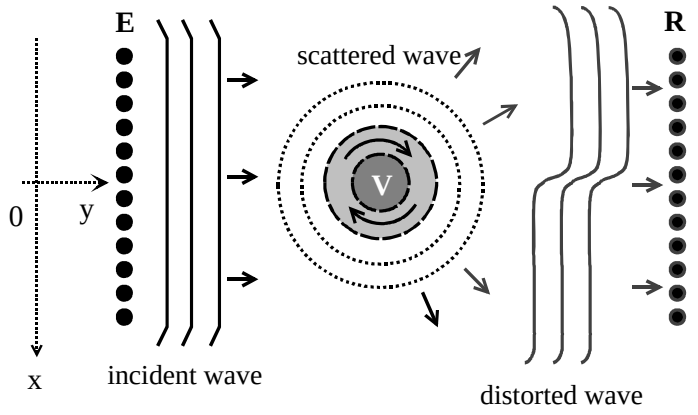

Fig. 2. Sound-flow interaction: the incident wave is emitted by the transducer array (E) and distorted by the flow velocity field and, depending on the vortex, scattered by the vortex core (V). The receiving array (R) records the pressure field transmitted through the vortex.

3.2 Measurement technique

A plane ultrasonic wave is emitted from a linear array of 64 piezzo-electric transducers with a pitch of 0.83 mm and with a central frequency of f =3.5 MHz (see fig. 2). The sound speed in water at rest is taken to be c =1480 m/s, which leads to a wavelength of λ =0.42 mm. A second array of 64 transducers, parallel to the emitters and about 30 cm apart, records the pressure field after one crossing of the vortex. The Mach number $M = u/c$ where u is a characteristic velocity of the vortex (for instance, the maximum orthoradial velocity) is of order $10^{-3}$and for the times-of-flight and for the propagation distances involved here, it can be considered that (i) the flow is frozen during the time of acoustic propagation, (ii) acoustic rays remain straight from a transducer array to another, and (iii) no frequency shift occurs for the incident wave.

A first experiment in the fluid at rest is performed to get some reference pressure signals. Those signals are then compared to the signals received after crossing the vortex: by taking the ratio of the Fourier transforms of the signals obtained in the presence of a vortex and in the fluid at rest, a phase and amplitude information is recovered on the wavefront distortion due to the crossing of the vorticity filament [12,3] . This information is a function of the position x of the receiver. Thus, with a single plane emission, the use of transducer arrays yields a spatial information on the flow along the x-axis. Let us also note that when the vortex is axisymmetric, the measurement depends only on the orthoradial component $v_\theta(r, z)$ of the velocity field (where r is the distance to the vortex center and z the position along the vortex axis) and carries no information on the longitudinal and radial components $v_z(r, z)$ and $v_r(r, z)$.

3.3 Acoustic data analysis

Figure 3 shows the typical phase and amplitude distortions averaged on 500 samples in the case of a stable vortex (for which the precession motion can be neglected). In spite of the low Mach number, the effect of the vortex on the incident wave is noticeable and precisely mesurable. Error bars correspond to the standard variation of the measurements and are due to (i) the weak instationarity of the flow, (ii) the vibrations of the experimental setup, and (iii) the electronic noise surrounding the experiment.

The main feature of the phase distortion Φ(fig. 3(a)) is the phase jump $\Delta\Phi = \Phi(x \geq 15 \text{ mm}) - \Phi(x \leq 15 \text{ mm})$ when crossing the vortex. This corresponds to the geometric advection of the acoustic wave by the vortex velocity field: depending on the side of the vortex it crosses, the wave is slowed down ($\Phi \leq 0$) or sped up ($\Phi \geq 0$) compared to the propagation in the fluid at rest. For an irrotational velocity field $v_\theta(r,z) = \Gamma/2\pi r$ far from the vortex core, the geometrical acoustics computation yields

$$\Delta\Phi = \frac{2\pi f}{c^2}\Gamma$$

where Γ is the vortex circulation . From the phase distortion Φ, we can thus deduce the position x_0 of the vortex center along the x-axis ($\Phi(x_0) = 0$) as well as the vortex circulation. In the case of figure 3, the phase jump yields $\Gamma = 145$ cm^2/s.

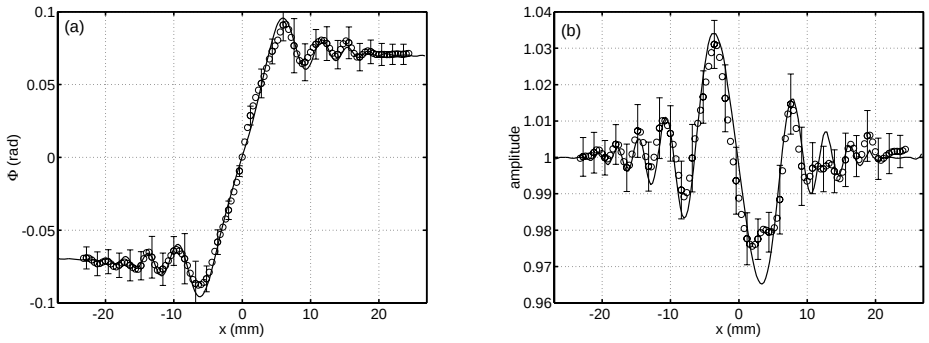

Fig. 3. Analysis of the mean distortion of a plane ultrasonic wave after crossing of a stretched vortex ($\Omega/2\pi$=1.7 Hz, D=80 mm, Q=5.6 L/min). (a) Phase distortion. (b) Amplitude distortion. The abscissa x is the transducer position along the receiver array. The origin $x = 0$ was arbitrarily taken as the position of the vortex center. Solid curves are the best theoretical fits of the data based on analytical calculations of sound scattering by a vortex for which Γ=145 cm^2/s and r_0=1.3 mm.

Another feature of the wavefront distortion is the presence of oscillations both on the phase (fig. 3(a)) and on the amplitude (fig. 3(b)) signals. Those oscillations

result from the interference between the wave scattered by the vortex core and the incident wave advected by the flow as soon as the core radius r_0 is smaller than a few λ (typically 5λ). In that case, analytical calculations [12] for a perfect plane wave generated at infinity and incident on a velocity field given by

$$v_\theta(r,z) = \frac{\Gamma}{2\pi r} \text{ for } r \geq r_0,$$

$$v_\theta(r,z) = r\omega \text{ for } r \leq r_0 \text{ with } \omega = \frac{\Gamma}{2\pi r_0^2}$$

allows to account very well for those oscillations by using the value of Γ measured above and by adjusting only the value of r_0. The fits shown in fig. 3 yield a circulation $\Gamma = 145 \pm 5$ cm^2/s and a core radius $r_0 = 1.3 \pm 0.5$ mm$\approx 3\lambda$. Even if r_0 is not known very precisely, it is important to note that this method allows some measurements inside a very small vortex core, which is not accessible to usual techniques.

4 Experimental results

We checked that the results presented below are weakly dependent on the position z of the transducer arrays along the vortex axis. Thus, the orthoradial velocity $v_\theta(r,z)$ is taken as independent of z [6].

4.1 Mean characteristics as a function of the control parameters

Figure 4 shows the vortex circulation Γ as a function of the control parameters: the rotation speed of the discs Ω, the distance between the discs D, and the total suction flowrate Q.

The scaling law obtained for $\Gamma(\Omega)$ (fig. 4(a)) with an exponent close to 3/4 differs from the $\sqrt{\Omega}$ scaling predicted and observed in confined geometries [8][16]. This scaling law together with pressure measurements allows to deduce scaling for $u_{\theta,max}$ and r_0 as a function of Ω [17]. The scaling law $\Gamma \propto D^{-1/2}$ (fig. 4(b)) for small values of D is qualitatively explained by the following energetic argument: the power dissipated in the volume of the vortex outside the boundary layers depends only on Ω and Q, thus $\int(\partial v/\partial r)^2 dV \sim \Gamma^2 D/r_0^2 = f(\Omega, Q)$, which leads to $\Gamma \propto D^{-1/2}$(assuming that r_0 is independent of Γ and D). Those first two results indicate that the geometry of our experiment gives rise to a vorticity filament which is noticeably different from a confined vortex where forcing by the Eckman layers is essential.

Finally, the weak linear dependence of Γ upon Q is similar to the one observed in confined vortices, which may indicate that the suction essentially plays a role in the boundary layers close to the discs. Complementary measurements, for instance of the stretching , could lead to a consistent model for a stretched vortex in an infinite medium.

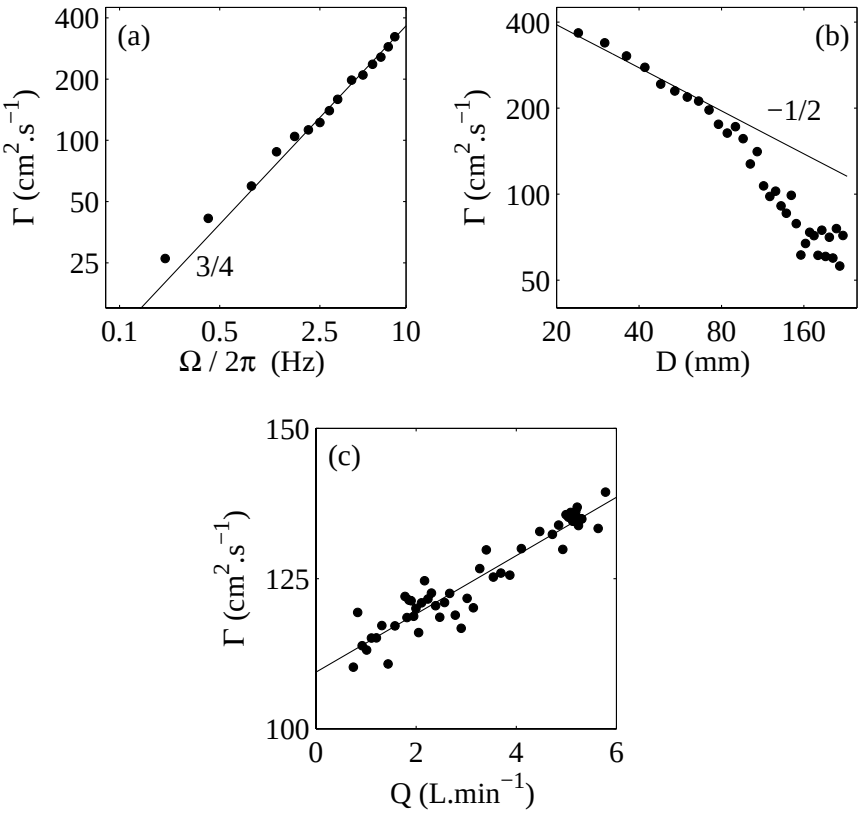

Fig. 4. Vortex circulation as a function of (a) the rotation speed of the discs Ω (for $D = 120$ mm and $Q = 3.0$ L/min), (b) the distance between the discs D (for $\Omega/2\pi = 1.7$ Hz and $Q = 5.6$ L/min), and (c) the suction flowrate Q (for $\Omega/2\pi = 1.7$ Hz and $D = 80$ mm).

4.2 Dynamical tracking of the vortex

The measurements presented above can also be performed on an unstable or non-stationary vortex, with a sampling frequency of about 30 Hz. This yields a dynamical tracking of the vortex position $x_0(t)$ and of its circulation $\Gamma(t)$. The measurement of the vortex size as a function of time is also possible but it implies to adjust r_0 in the analytical calculation for each sample. Our results are qualitatively similar to previous observations on a confined vorticity filament [10,9,18].

- Example of transitory regime: figure 5 shows dynamical measurements performed on a stable vortex for which the sign of the disc rotation is abruptly changed at time t_0. After the perturbation, the vortex is formed far from the rotation axis of the discs ($x_0 = 0$) and oscillates and stabilizes around

$x_0 = 0$ in about 10 s. The circulation goes from Γ_0 to -Γ_0 in the same time interval and its behaviour is well modelled by an exponential relaxation with a characteristic time of about 5 s.

- Precession motion and 2D trajectory of the vortex: a slight modification of the measurement setup leads to the trajectory of the vortex in the incidence plane of the acoustic wave. Here, we use a circular array of 128 transducers and of diameter 20 cm that completely surrounds the vortex. Three spherical waves are simultaneously emitted from three transducers at 120^{O} on the circular array. The coordinates $(x_0(t), y_0(t))$ are then computed by triangulation from the three angles corresponding to the zero phase-shifts of the incident spherical waves. An example of such measurements is shown in figure 6. A small precession frequency f_p is clearly measurable from the time series $x_0(t)$ and $y_0(t)$ (fig. 6(a) and (b)) and the trajectory of the vortex is close to a circle of radius r_p travelled in the same direction as that of the disc rotation. The radius of the precession increases with the distance between the discs and the motion is truly periodic only above a certain value of D of about 14 cm (fig. 6(c) and (d)).

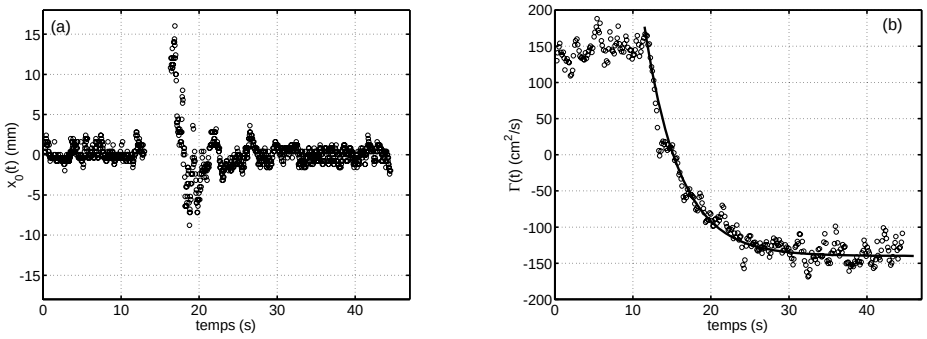

Fig. 5. Transitory regime after changing the sign of the disc rotation at time $t_0 = 12$ s ($\Omega/2\pi = 1.7$ Hz, $D = 80$ mm, $Q = 5.6$ L/min). (a) Vortex abscissa $x_0(t)$. (b) Vortex circulation $\Gamma(t)$; the solid line is an exponential fit $2\Gamma_0(\exp((t_0-t)/\tau)-1/2)$ for $t \geq t_0$, with $\tau = 4.5$ s.

5 Conclusions and perspectives

A new expriment was set up, that allows to investigate systematically the effects of the control parameters on both the mean characteristics and on the dynamics of a stretched vortex in a non-confined medium. The behaviour of such a vortex turns out to be slightly different from that observed in confined geometries and may be more representative of the characteristics of the vorticity filaments in turbulent flows.

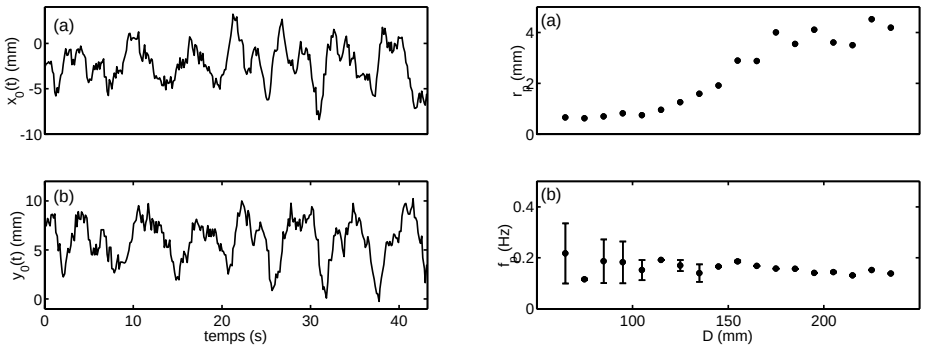

Fig. 6. Precession motion of the vortex ($\Omega/2\pi = 2.5$ Hz, $D = 165$ mm, $Q = 5.6$ L/min). Vortex coordinates (a) $x_0(t)$ and (b) $y_0(t)$ obtained by triangulation. (c) Radius r_p and (d) frequency f_p of the precession as a function of the distance between the discs D.

Our acoustic method based on the use of transducer arrays is non-invasive and yields directly a spatial information even in the core of a vortex which is only a few acoustic wavelengths. This method allows fast dynamical measurements and the sampling frequency could be increased from 30 Hz to about 1 kHz in the next future.

Finally, the systematic use of spherical waves emitted from a circular transducer array surrounding the vortex is under study, in order to improve the precision on the vortex core measurement and to allow a 2D tomography of the flow.

References

1. Cadot O., Douady S., Couder Y., *Phys. Fluids*, **7**, 630–646 (1995).
2. Brachet M.-E., *Fluid Dyn. Res.*, **8**, 1–8 (1991).
3. Jimenez J., *Phys. Fluids*, **4**, 652–654 (1991).
4. Belin F., Maurer J., Tabeling P., Willaime H., *J. Phys. II France*, **6**, 573–583 (1996).
5. Chainais P., Abry P., Pinton J.-F., submitted to *Phys. Fluids* (1999).
6. Bottausci F., Petitjeans P., Wesfreid J.E., Maurel, A. Manneville, S., Structure and Dynamics of vortices, Springer-Verlag, (2000)
7. Roux S., Muzy J.-F., Arneodo A., to appear in Eur. Phys. J. B (1999).
8. Mory M., Yurchenko N., *Eur. J. Mech. B*, **6**, 729–747 (1993).
9. Andreotti B., Maurer J., Couder Y., Douady S., *Eur. J. Mech. B*, **17**, 451–470 (1998).
10. Pinton J.-F., Chillà F., Mordant N., *Eur. J. Mech. B*, **17**, 535–547 (1998).
11. Petitjeans Ph., Robres J.-H., Wesfreid J.-E., Kevlahan N., *Eur. J. Mech. B*, **17**, 549–560 (1998).
12. Roux Ph., de Rosny J., Tanter M., Fink M., *Phys. Rev. Lett.*, **79**, 3170–3173 (1997).

13. Labbé R., Pinton J.-F., *Phys. Rev. Lett.*, **81**, 1413–1416 (1998).
14. Manneville S., Maurel A., Roux Ph., Fink M., *Eur. Phys. J. B*, **9**, 545–549 (1999).
15. Manneville S., Robres J.-H., Maurel A., Petitjeans Ph., Fink M., *Phys. Fluids*, **11**, 3380–3389 (1999).
16. Andreotti B., Ph. D thesis, University Paris VII (1999)
17. Moisy F, Petitjeans P, Structure and Dynamics of vortices, Springer-Verlag (2000)
18. Wunenburger R., Andreotti B., Petitjeans Ph., soumis à *Exp. Fluids* (1999).
19. Winters K. B., Rouseff, *IEEE Ultrason. Ferroelec. Freq. Control*, **40**, 26–33 (1993).
20. Johnson S. A., Greenleaf J. F., Tanaka M., Flandro G., *ISA Trans.*, **16**, 3–15 (1997).
21. Landau L. D., Lifshitz E. M., *Fluid Mechanics*, 2nd edition, chap. 8, (MIR, Moscou, 1989).
22. Salant R. F., *J. Acoust. Soc. Am.*, **46**, 1153–1157 (1969).
23. Georges T. M., *J. Acoust. Soc. Am.*, **51**, 206–209 (1971).
24. Lighthill M. J., *Proc. R. Soc. London A*, **211**, 564–587 (1952).
25. Kraichnan R. H., *J. Acoust. Soc. Am.*, **25**, 1096–1104 (1953).
26. Fetter F. L., *Phys. Rev. A*, **136**, 1488–1493 (1964).
27. Fabrikant A. L., *Sov. Phys. Acoust.*, **29**, 152–154 (1983).
28. Sakov P. V., *Acoust. Phys.*, **39**, 280–282 (1993).
29. Lund F., Rojas C., *Physica D*, **37**, 508–514 (1989).
30. Baudet C., Ciliberto S., Pinton J.-F., *Phys. Rev. Lett.*, **67**, 193–195 (1991).
31. Pinton J.-F., Laroche C., Fauve S., Baudet C., *J. Phys. II France*, **3**, 767–773 (1993).